Article

Analysis on Characteristics of Mixed Traffic Flow with Intelligent Connected Vehicles at Airport Two-Lane Curbside Based on Traffic Characteristics

Xin Chang [1] , Weiping Yang [1], Yao Tang [1], Zhe Liu [2],* and Zheng Liu [1]

[1] School of Transportation Science and Engineering, Civil Aviation University of China, Tianjin 300300, China; xchang@cauc.edu.cn (X.C.); 13643775041@163.com (W.Y.)

[2] Transport Planning and Research Institute, Ministry of Transport, Beijing 100028, China

* Correspondence: liuzhe@tpri.org.cn

Abstract

With the growing adoption of connected and autonomous vehicles (CAVs), their market penetration is expected to rise. This study investigates the mixed traffic flow dynamics of human-driven vehicles (HDVs) and CAVs at airport terminal curbsides. A two-lane parking simulation model is developed, integrating the intelligent driver model, PATH-calibrated cooperative adaptive cruise control, and a degraded adaptive cruise control model to capture different driving behaviors. The model accounts for varying time headways among HDV drivers based on their information acceptance levels and imposes departure constraints to enhance safety. Simulation results show that the addition of CAVs can significantly increase the average speed of vehicles and reduce the average delay time. Two metrics are inversely proportional. Specifically, as illustrated by a curbside length of 400 m and a parking demand of 1300 pcph, when the CAV penetration rate p is 10%, 30%, 50%, 70%, and 100%, respectively, compared to $p = 0$, the average traffic flow speed increases by 1.7%, 6.4%, 15.0%, 27.2%, and 48.7%, respectively. The average delay time decreases by 2.8%, 6.4%, 10.5%, 13.5%, and 20.0%, respectively. Meanwhile, CAVs and HDVs exhibit consistent patterns in terms of parking space utilization: the first stage (0–30% of parking spaces) showed a stable and concentrated trend; the second stage (30–70% of parking spaces) showed a slow downward trend but remained at a high level; the third stage (70–100% of parking spaces) showed a rapid decline at a steady rate.

Keywords: mixed traffic flow; two-lane curbside; car-following model; connected vehicle; penetration rate

1. Introduction

The international civil aviation industry has undergone rapid expansion in recent decades, establishing air transportation as a critical mode of travel for both domestic and international routes. According to the International Air Transport Association's preliminary annual report on global aviation statistics, passenger demand in 2024 demonstrated significant growth, with a 10.4% year-on-year increase. This recovery not only reflects a robust rebound but also exceeds pre-pandemic levels by 3.8% [1]. The continuous increase in air travelers has intensified pressure on airport infrastructure and operational efficiency. Researchers have emphasized that rising passenger volumes have led to increased demand for airport services, increased ground congestion around airports, and increased flight

delays [2–4]. Furthermore, these challenges raise security concerns for travelers and complicate airport management, necessitating strategic interventions to ensure sustainable aviation growth.

Most researchers focus on how to properly plan and design curbsides to address ground congestion around airports and flight delays. Increasing curbside capacity is a popular method. Parizi et al. conducted a comprehensive investigation into airport terminal curbside design by analyzing passenger demand patterns, and their research led to the development of a novel single-lane parking simulation model for evaluating curbside operational capacity [5]. Then, Lu et al. proposed a two-lane curbside capacity formula considering internal and external mobility based on a single road parking model, and the results showed that the curbside capacity could be effectively improved by adding other lanes [6]. Zhang found that curbside capacity can be improved by optimizing the form of berth arrangement [7]. However, all these articles estimated the curbside length by empirical values or formulas, which led to changes in results that were difficult to explain. After that, the research focus turned to simulation modeling, aiming to explain the impact of traffic flow on curb capacity from a microscopic perspective. Various researchers conducted theoretical analysis through queuing models and established a curbside capacity calculation model with vehicle arrival, stopping, and departure times as indicators [8–12]. Chen et al. analyzed the impact of lane width, number of vehicles, stopping mode, and other factors on the curbside capacity; based on the queuing theory and the influence coacceptable method, they established a capacity calculation model considering the time of passenger alighting and vehicle stopping time [10]. Liu et al. considered the role of vehicles and added the constraints of the car-following (CF) model to establish a two-lane parking model, which solved the problem of calculating the number and length of parking spaces, the study also showed that even if all the parking needs were satisfied, a certain amount of delay would be incurred [11]. Harris et al. developed a mesoscopic simulation model to evaluate the effectiveness of management policies for addressing increasing airport curbside congestion. The model simulates scenarios of parking allocation, increased passenger demand, and dwell time constraints. The results show that different management strategies with different impacts on various scenarios can significantly reduce the waiting time for passengers and vehicles [12]. In summary, existing studies largely rely on empirical formulas, leading to insufficient accuracy; some static or simplified assumptions overlook real traffic fluctuations and passenger behavior differences, and there is also a lack of systematic evaluation across multiple scenarios and strategies. However, the previous work has laid a better foun-dation for the study of the terminal curbside.

The findings of these studies can provide theoretical guidance for curbside design in new airport construction. However, applying this approach to improve curbside capacity at existing airports may not be advisable. Terminal reconstruction constitutes a capital-intensive undertaking that requires substantial financial investment and may temporarily disrupt airport operations. During the expansion of the terminal forecourt at London Heathrow Airport T5, the newly added ride-hailing zone initially caused short-term traffic delays for pick-up and drop-off vehicles. Meanwhile, some passengers had to take temporary detour routes, increasing their walking distance. The development of connected and autonomous vehicles (CAVs), especially adaptive cruise control (ACC) and cooperative adaptive cruise control (CACC) systems [13–15], allows real-time tracking of vehicle dynamics, thereby enhancing car-following efficiency. The efficacy of CAVs in improving transportation outcomes has been well-documented, with substantial evidence supporting their role in accident reduction, traffic flow optimization, and safety improvement [16–19]. However, because of the complexity of autonomous driving technology and relevant policies, as well as the challenge of changing people's habits and perceptions towards traditional

driving modes, it may take several decades for CAVs to achieve high market penetration rate. Consequently, a transitional phase featuring a new type of mixed traffic flows that include both CAVs and human-driven vehicles (HDVs) is expected to persist in airport curbside for the foreseeable future [20].

Research on the characteristics of mixed traffic flow has become relatively mature. Yao et al. used different car-following models to describe the behaviors of high-density vehicles, CACC vehicles, and ACC vehicles, respectively. This study assessed highway safety performance in mixed traffic conditions through a comprehensive evaluation framework incorporating multiple safety indexes and heterogeneous traffic flow stability analysis across varying CAV penetration rates levels. The results of the study indicate that appropriate deployment of CAVs can significantly improve traffic flow stability and road safety [21]. Pan et al. systematically examined the influence of CAVs on heterogeneous traffic systems, focusing particularly on congestion mitigation and traffic efficiency enhancement. Their analysis reveals that CAVs can substantially diminish human-factor uncertainties in driving behaviors, leading to measurable improvements in traffic stability, safety performance, and overall system sustainability [22]. Amirgholy and Nourinejad proposed a novel CAV control framework, where CAVs act as platoon leaders to coordinate the movement of HDVs at road intersections, enabling macroscopic optimization of mixed traffic flow. By establishing a stochastic model and employing a Markov-based approach, they characterized the randomness in multi-lane intersection platoon coordination. Results demonstrate significant improvements in both intersection capacity and network efficiency through the proposed approach, achievable even with minimal CAV penetration rates [23]. Cen et al. developed a heterogeneous traffic flow framework grounded in the intelligent driver model (IDM) to investigate the interactive dynamics between CAVs and HDVs. By incorporating V2V communication, they constructed a Markov chain model to describe vehicle distribution patterns. Numerical simulations demonstrated that increasing CAV penetration rates can significantly enhance traffic flow stability and road capacity [24]. In summary, existing studies on mixed traffic flow models are mostly limited to typical scenarios and lack adaptation to the specific conditions of roads around airport terminals. Some models are based on idealized assumptions, failing to fully capture complex factors such as traffic fluctuations, disturbances caused by passenger boarding and alighting, and driving behavior differences in mixed traffic. Simulation analyses also lack systematic sensitivity evaluations for various management strategies, changes in traffic demand, and unexpected events, making it difficult to comprehensively assess the robustness and applicability of the models across diverse scenarios. Nevertheless, these studies offer valuable insights for optimizing road capacity around airport terminals and mitigating traffic congestion.

CAVs have already been implemented in terminal curbside operations at major international airports. Representative cases include the following: London Gatwick Airport partnered with British autonomous software company Oxbotica in 2018 to conduct trials of electric autonomous vehicles, with the aim of enabling seamless transportation of staff between the North and South Terminals; The Beijing High-Level Autonomous Driving Demonstration Zone Working Office, in collaboration with Baidu and Pony.ai, successfully completed trial runs of autonomous vehicles in 2023. These vehicles were used for picking up and dropping off passengers at the terminal building of Daxing International Airport and conducting internal transfers within public areas; New York's John F. Kennedy International Airport has launched several autonomous vehicle pilot projects to improve passenger transportation efficiency. In July 2024, the Port Authority of New York and New Jersey launched an autonomous shuttle pilot project offering free transportation services. However, there is still a gap in this area of research on the characteristics of the new mixed traffic flow composed of HDVs and CAVs with the airport terminal curbside as the driving

environment; fewer studies provide a good theoretical basis for future airport curbside design and traffic management.

In this study, we attempt to explore the characteristics of a new type of mixed traffic flow, aiming to provide theoretical guidance for airport curbside design. To achieve this target, this paper establishes a two-lane simulation model. We take the car-following model as a constraint and consider the impact of the HDV driver's driving experience on the vehicle's information reception ability. Moreover, to avoid the occurrence of dangerous accidents after the vehicle completes parking services, we limit its departure conditions. Using these methods, we simulated the characteristics of new mixed traffic flow in different scenarios, reproducing the entire process of vehicle arrival, parking service, and departure. Thus, we analyzed the impact of the penetration rate of connected vehicles on the traffic efficiency of traffic flow, delay time, and parking space utilization.

2. Research Scenario and Framework

2.1. Curbside Characteristics

The terminal curbside serves as a critical connection platform, facilitating passenger and luggage transfers between ground transportation and the airport terminal. It accommodates vehicle pick-up and drop-off operations, ensuring efficient passenger flow and baggage handling. The different types of airport terminal curbsides are inconsistent; the physical environment selected for simulation in this paper is a two-lane departing curbside. Since single-lane curbsides are rare in practice, with most vehicle service points located near terminals and traffic concentrated internally, the two-lane configuration serves as a basis for analyzing multi-lane scenarios. In most airport configurations, the departure curbside is vertically segregated from the arrival curbside, typically positioned on the upper level to facilitate passenger drop-off before terminal entry and flight boarding.

Figure 1 illustrates the conventional lateral layout of departure curbside operations. The vehicle operation process is divided into three distinct phases:

- The vehicle enters the curbside area in the direction of the traffic flow indication direction;
- The vehicle performs stop and drop off service within the designated drop-off lane;
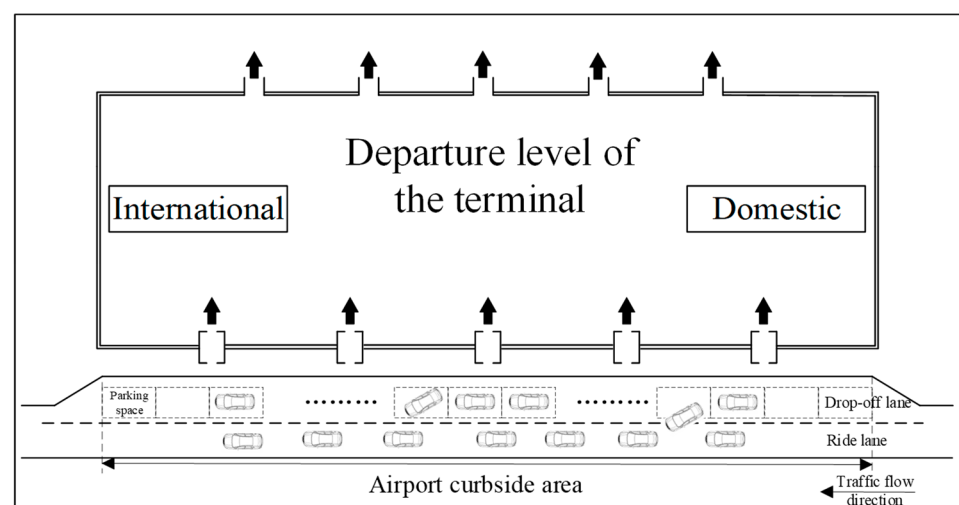- The vehicle exits through the ride lane after service is completed.

Figure 1. Classic departure curbside layout.

There are different types of vehicles that use airport terminal curbsides, which may include taxis, public buses, airport buses, and private cars. Empirical studies confirm that

private cars dominate airport access patterns. This prevalence stems from factors such as convenience, lack of competitive public transit alternatives, and passenger preferences for door-to-door service [25,26]. This phenomenon generates significant parking demand and leads to frequent congestion on the terminal curbside. Extensive studies have been conducted to examine the distinct parking behaviors of various vehicles at airport terminal curbside, with particular focus on dwell time patterns and space utilization [27–29]. For example, Chen et al. investigated the airport departure curbside traffic characteristics to obtain the parking time of different vehicles using Beijing Capital International Airport as the research object [10]. Yang et al. used video to record the behavioral characteristics of drop-off taxis at the terminal curbside, along with detailed counts of the taxis' stopping times [29]. Referring to Chen and Yang, the space occupation and dwell time at the departure curbside for different types of vehicles are shown in Table 1. There is a common view that private cars and airport buses are recommended to load passengers in parking lots near airports; in other words, these two types of vehicles are not allowed to reach the airport terminal curbside in most airports.

Table 1. Comparative analysis of vehicle parking characteristics: space occupation and dwell time.

Curbside	Vehicle	Space Occupation	Dwell Time
	Bus	20 m	120 s
Departing curbside	Airport bus	14 m	121 s
	Taxi	8 m	50 s

2.2. Mixed Traffic Flow Configurations

The simulation framework incorporates mixed traffic conditions with both HDVs and CAVs operating simultaneously at the terminal curbside. Vehicle interactions are modeled using car-following theory, where the lead vehicle is specifically defined as the closest preceding vehicle to each follower in the traffic flow.

The intelligent driver model (IDM) was selected to simulate human-driven vehicle (HDV) dynamics, as it effectively captures both free-flow acceleration characteristics and congestion-induced deceleration behavior while maintaining collision-free operation. Model validation against empirical data demonstrates strong agreement with real-world driving patterns [30]. To simulate the experiment close to the real scenario, we consider the effect of the driver's driving experience on the vehicle's information acceptance ability and categorize HDVs into radical, stable, and cautious types [31]. Some studies indicate that stable drivers are more often present in CAVs [32]. We choose the ratio of 1:3:1 in this experiment, which is mainly reflected in the different time headways from the lead vehicle.

CACC vehicles can utilize inter-vehicle communication technology to implement communication with the front vehicle, but the realization of CACC vehicle functions requires the front vehicle to install communication equipment. In other words, if the lead vehicle of CAV is CAV, the vehicle is controlled by CACC; on the contrary, if it is HDV, CACC degrades to ACC, so the interaction of information is realized by the ACC and the CACC vehicle constituting the connected vehicle fleet. Due to the limited length of the curbside, it is assumed that inter-vehicle communication can be realized within the length of the curbside, and the vehicle distribution is shown in Figure 2.
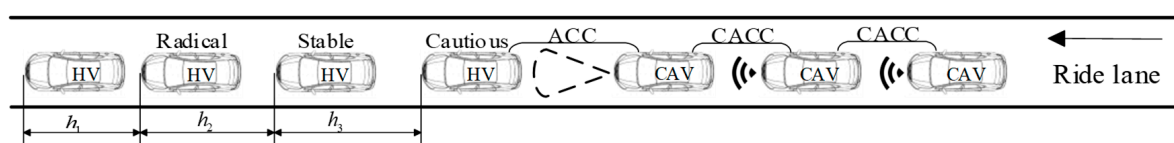

Figure 2. Schematic diagram of the vehicle distribution.

2.3. Research Framework for the Operating Characteristics of Mixed Traffic Flow

This study focuses on mixed traffic flow with the participation of CAV vehicles, using the airport terminal departure-level curbside as the simulation model environment to explore the operational characteristics of mixed traffic flow. The research framework is shown in Figure 3. In Section 3.1, the models required for the simulation experiments are constructed, including the vehicle following model and the lane change model. Section 3.2 designs the simulation program, based on the models built in Section 3.1, with four programs: selection of the car-following model, parking space status handling, vehicle state handling, and the principles of the simulation experiment. Section 4 presents the analysis of the simulation results, where different simulation scenarios are built based on curbside length, CAV penetration rate, and parking demand. Evaluation metrics, including average vehicle speed, average vehicle delay, and parking space utilization, are used to analyze the performance of the three indicators in different scenarios.
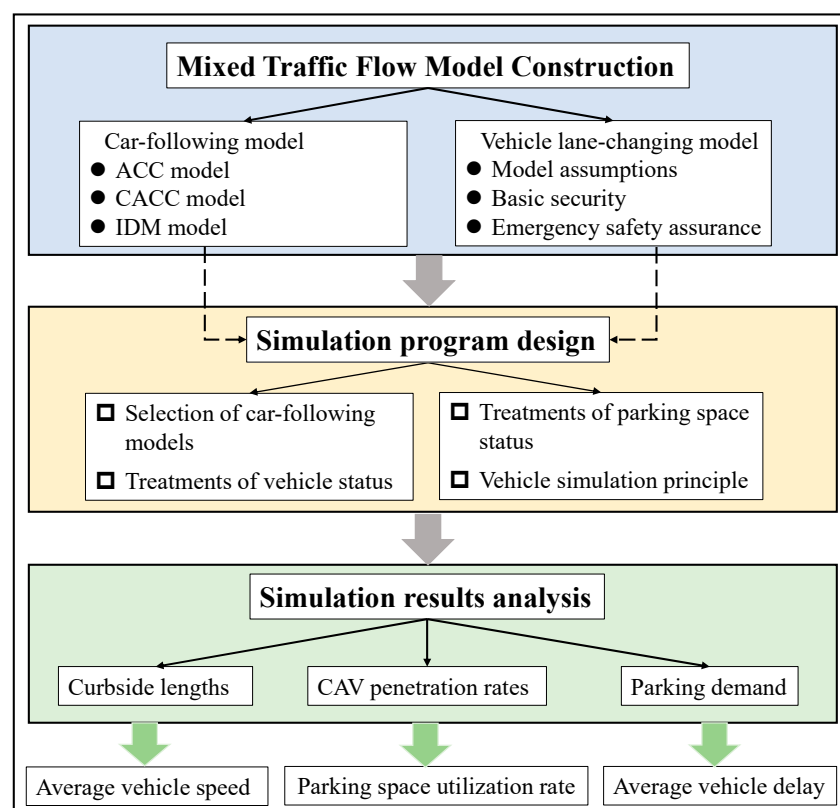

Figure 3. Research framework for the operating characteristics of mixed traffic flow.

3. Method

3.1. Model Construction

3.1.1. Car-Following Model

The IDM model considers the interaction between vehicles and can predict the behavior of traffic flow more accurately. Meanwhile, it can distinguish the responsiveness of different types of drivers to connection information when describing the driving behavior of HDVs [33–36], so it has been widely used by researchers with the model in Equation (1). For CAVs, the motion state of each vehicle is controlled by the CACC model only when the lead vehicle is also a CAV. Extensive research conducted by the PATH Laboratory at UC Berkeley has demonstrated the efficacy of this modeling approach through field experiments, particularly in examining CAV following behavior under various traffic conditions [37,38]. The CACC is given by Equation (2). For CAVs, when the lead vehicle is an

HDV, CACC degrades to ACC, and the vehicle motion is controlled by the ACC model. The ACC vehicle following the model proposed by the UC Berkeley team through the study of ACC vehicles is generally recognized [39,40], which is shown in Equation (3).

$$a_{IDMi} = a_{mi} \left[1 - \left(\frac{v}{v_0} \right)^\delta - \left(\frac{s_0 + vh_i + v\Delta v (2\sqrt{a_{mi}b_i})^{-1}}{h - l} \right)^2 \right] \tag{1}$$

$$a_{CACC} = \frac{k_p(h - l - s_0) - k_p t_c v + k_d v}{\Delta t + k_d t_c} \tag{2}$$

$$a_{ACC} = k_c[h - Tv - l - s_0] + k_v \Delta v. \tag{3}$$

where a_{IDMi}, a_{CACC}, and a_{ACC} are the accelerations under different car-following models, respectively. a_{mi} is the maximum desired acceleration, v_0 is the free flow speed, v is the vehicle speed, Δv is the vehicle and the lead vehicle speed difference, δ is the acceleration component, h_i is the safety time headway, b_i is the absolute maximum desired deceleration, and h is space headway. l is the vehicle length, and the value is chosen as 5 m. s_0 is the minimum safety distance and the value is chosen as 2 m. In addition, $i = 1$ denotes type radical, $i = 2$ type stable, and $i = 3$ type cautious. We use different safety time headways to distinguish between the driving styles of different drivers ($h_1 = 0.8$ s, $h_2 = 1.0$ s, $h_3 = 1.5$ s). k_p and k_d are the control error parameters, t_c is the desired time headway, k_v and k_c are the control error parameters, and T is the desired time headway. The parameters of each type of model are shown in Table 2.

Table 2. Model parameters for IDM, ACC, and CACC.

Type	Parameter	Value
IDM	b_i	2.0 m/s^2
	a_{mi}	2.17 m/s^2
	v_0	11.1 m/s
	δ	4
ACC	k_p	0.45
	k_d	0.25
	t_c	0.8 s
	Δt	0.01 s
CACC	k_c	0.23
	k_v	0.07
	T	1.1 s

3.1.2. Analysis of Vehicle Lane-Changing Conditions

When the vehicle completes the parking service, the vehicle chooses a suitable moment to leave the parking space and drive into the ride lane, eventually leaving the curbside. Vehicles leaving the drop-off lane under normal situations need to be conditioned. Meanwhile, we have considered the occurrence of real-life emergencies in our simulation model. Based on these two points, we make the following assumptions when vehicles enter the ride lane:

- We ignore the lateral motion of the vehicle and assume that the vehicle enters the destination lane in a translational attitude at one instant;
- When an emergency occurs in the lead vehicle, the back vehicle can immediately sense and act, assuming a reaction time of 0 for the driver;
- The vehicle brakes well and brakes at maximum acceleration;

- The occurrence of an emergency is only considered when a vehicle leaves the drop-off lane and is related to the departing vehicle;
- Vehicles entering the ride lane drive at the speed of the lead vehicle as the desired speed, and when there is no lead vehicle, the vehicle speed is 0.

In this section, we denote a vehicle that leaves the drop-off lane and enters the ride lane as Car_n. The two situations of whether Car_n. has the lead vehicle are discussed by us. The purpose is to avoid vehicle collisions in the events of vehicle emergencies. When the Car_n has no lead vehicle, the normal conditions for departure satisfy Equation (4). Figure 4 shows an extreme case of an emergency in which the Car_n enters the ride lane and remains stationary. At this time, the back vehicle senses the Car_n failure and brakes immediately until the speed is 0. The change in position of the vehicle behind the Car_n is represented by Equation (5). The distance between the two vehicles is denoted by d_{safe}. When $d_{safe} > 0$, the back vehicle can react to the emergency situation of Car_n timely to avoid the collision of the two vehicles. This case satisfies Equation (6), and the Car_n can enter the ride lane.

$$x_{(n,t,1)} - x_{(back\_n,t,2)} > l \tag{4}$$

$$x_{(back\_n,t+1,2)} = x_{(back\_n,t,2)} + \frac{v^2_{(back\_n,t)}}{2a_{\max}} \tag{5}$$

$$x_{(n,t,1)} - x_{(back\_n,t+1,2)} > l \tag{6}$$

where $x_{(n,t,1)}$ denotes the position of Car_n in the drop-off lane at time t, $x_{(back\_n,t,2)}$ denotes the position of the vehicle closest to the back of Car_n in the direction of traffic flow in the ride lane at time t, $v_{(back\_n,t)}$ denotes the speed of the vehicle closest to the back of Car_n in the direction of traffic flow in the ride lane at time t, and $a_{\max}$ denotes the maximum acceleration of the vehicle during deceleration braking.
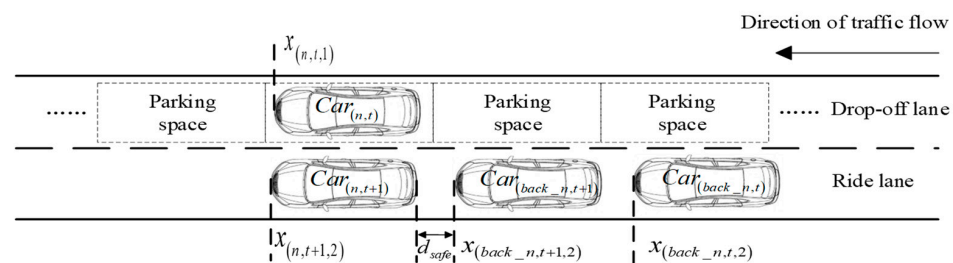

Figure 4. Analyzing conditions for collision avoidance in an extreme case of no lead vehicle.

When the Car_n has the lead vehicle, for normal conditions, the Car_n satisfies Equations (4) and (7) and can enter the ride lane. Since the Car_n has the lead vehicle, the Car_n enters the ride lane at the same speed as the lead vehicle. Therefore, when an emergency occurs in the lead vehicle, the Car_n and the lead vehicle brake together at the same time, and a collision between the two vehicles does not occur. In Figure 5, we show an extreme case in which the Car_n brakes as an emergency occurs in the Car_n. Meanwhile, the back vehicle senses the position of the Car_n and reacts with braking. The change in position of the Car_n and the back vehicle is represented by Equation (8). The final distance between the two vehicles at rest is denoted by d_{safe}, and when $d_{safe} > 0$, it can avoid a collision between the two vehicles. In this case, the Car_n satisfies Equations (4), (7) and (9), and the Car_n is able to drive into the ride lane.

$$x_{(head\_n,t,2)} - x_{(n,t,1)} > l \tag{7}$$

$$
\begin{cases}
x_{(n,t+1,2)} = x_{(n,t,1)} + \dfrac{v^2_{(head\_n,t)}}{2a_{\max}} \\[2mm]
x_{(back\_n,t+1,2)} = x_{(back\_n,t,2)} + \dfrac{v^2_{(back\_n,t)}}{2a_{\max}}
\end{cases}
\tag{8}
$$

$$
x_{(n,t+1,2)} - x_{(back\_n,t+1,2)} > l
\tag{9}
$$

where $x_{(head\_n,t,2)}$ denotes the position of the nearest vehicle in front of Car$_n$ in the direction of traffic flow in the ride lane at time t. Equation (4) is to ensure that Car$_n$ enters the ride lane and the vehicle in front has enough distance. Equation (7) indicates that Car$_n$ enters the ride lane, and the vehicle behind will not collide at the next moment.
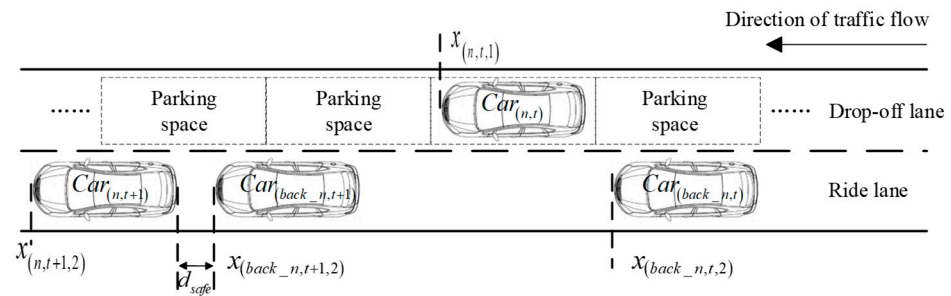

Figure 5. Analyzing the conditions for collision avoidance in an extreme case with the lead vehicle.

3.2. Simulation Program Design

3.2.1. Selection of Car-Following Models

The simulation environment accounts for car-following model effects on all vehicles except the first vehicle at the curbside. In addition, the simulation experiment has five different types of vehicles, and they are controlled by different car-following models, respectively. Therefore, this section provides an explanation for the selection of car-following models in the vehicle simulation process: this paper constructs the model in MATLAB to realize, three different HDVs in the simulation experiment are in the form of numbers, and the CAVs can select the appropriate model through the type of the lead vehicle. The specific choice of the car-following models is shown in Figure 6. Car$_n$ denotes the n-th vehicle. $a_{(n,t)}$ indicates the acceleration of Car$_n$ at the moment of t. Car$_n$ = I means that the Car$_n$ belongs to vehicle type I (I = 1 denotes type radical, I = 2 type stable, and I = 3 type cautious).
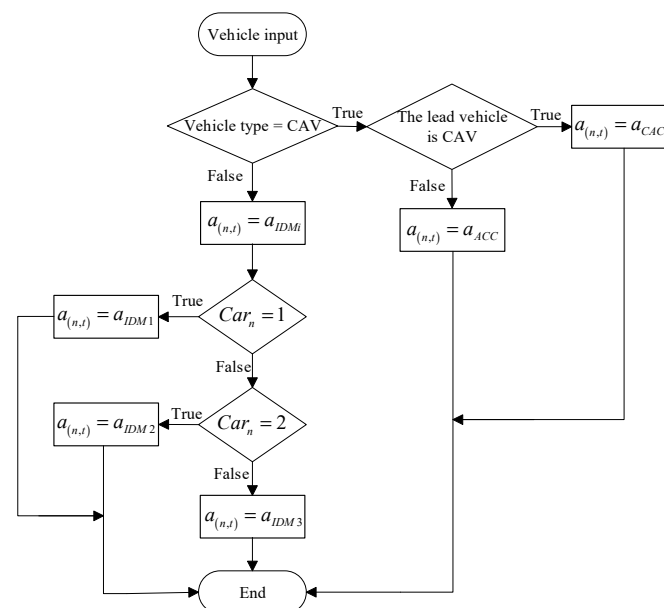

Figure 6. The logic of the car-following model selection procedure.

3.2.2. Treatments of Vehicle Status

This paper selects different curbside lengths to simulate mixed traffic flow in different scenarios. When the length of the curbside is short, there will be some vehicles leaving the curbside without stopping for service. The two modes of vehicles leaving the curbside are shown in Figure 7. Since the parking service of vehicles is performed at the curbside, and vehicles are in simple linear motion before reaching the curbside, only the status of vehicles after reaching the curbside is considered. We set up five statuses: arriving and car-followed (ACF), arriving and free-running (AFR), arriving and braking (AB), arriving and parking (AP), and arriving and leaving (AL). $S_{(n,t)} = I$ denotes the status of Car_n at time t, and the status of the vehicle is summarized in Table 3. Notice that AB status occurs when the vehicle is about to pull into a parking space, and AP means that the vehicle is in parking service.
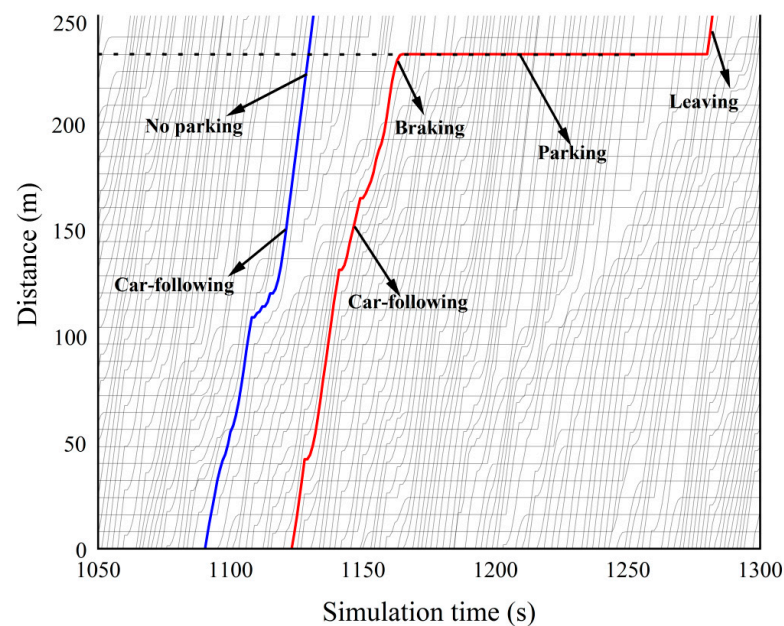

Figure 7. The temporal and spatial distribution of vehicle trajectories, where the red lines represent trajectories with parking, and the blue lines represent trajectories without parking.

Table 3. Statuses of vehicles.

Vehicle Status	Substitute Mode
Arriving and car-followed (ACF)	$S_{(n,t)} = 1$
Arriving and free-running (AFR)	$S_{(n,t)} = 2$
Arriving and braking (AB)	$S_{(n,t)} = 3$
Arriving and parking (AP)	$S_{(n,t)} = 4$
Arriving and leaving (AL)	$S_{(n,t)} = 5$

In the simulation experiment, the speed and position of the vehicles are updated as shown in Equation (10). The acceleration follows the following principle: when Car_n is in the AFR status, the vehicle drives with the maximum acceleration. When Car_n is in ACF status, $a_{(n,t)}$ follows the principle shown in Figure 3. The acceleration of the vehicle in status AB is calculated by Equation (11). When the i-th parking space is the nearest free parking space in front of Car_n, it is calculated whether $A_{(n,t)}$ is within the range of a_{brake}. If it is within its range, the calculation results in the acceleration of the Car_n in the AB status.

If it is not, the Car_n continues to follow the vehicle. The change in vehicle status is shown in detail in Figure 7.

$$\begin{cases} v_{(n,t)} = v_{(n,t-1)} + a_{(n,t)} \cdot t \\ x_{(n,t)} = x_{(n,t-1)} + v_{(n,t)} \cdot t \end{cases} \tag{10}$$

$$A_{(n,t)} = v_{(n,t)}^2 / 2x_{(n,t)} \tag{11}$$

where $a_{(n,t)}$, $v_{(n,t)}$, and $x_{(n,t)}$ are the acceleration, speed, and position of Car_n, respectively, at time t. a_{brake} is the range of acceleration of Car_n in AB status, which takes the values 1.45–2.25 m/s^2, a comfortable and feasible [41–44].

3.2.3. Treatments of Parking Space Status

To be able to clearly explain the principle of simulation. We set up three kinds of parking space statuses: target parking space (TPS), parking space locking (PSL), and parking space unlocking (PSU). The status of the parking space is summarized in Table 4. $M(i)$ denotes the status of the i-th parking space. When a parking space is in the PSU status, it means that a vehicle completes the parking service and satisfies the condition of leaving the drop-off lane. If the i-th parking space is the nearest free parking space in front of the Car_n, then the status of this parking space is TPS. Notice that the Car_n at this moment can be many vehicles. When the status of a parking space changes from TPS to PSL status, it means that one of the many vehicles is about to park in the parking space. The PSL status is realized in relation to the $A_{(n,t)}$ of the vehicle. When the vehicle departs from the parking space, the status of the parking space is the PSU status. The detailed process is shown in Figure 8. The parking spaces are ranked according to the direction of traffic flow, with the first space denoted by 1 and continuing. $Car_{(n,i,t)}$ denotes the i-th parking space of Car_n at time t.

Table 4. Statuses of the parking spaces.

Parking Space Status	Substitute Mode
Target parking space (TPS)	$M(i) = TPS$
Parking space locking (PSL)	$M(i) = PSL$
Parking space unlocking (PSU)	$M(i) = PSU$

3.2.4. Simulation Principle

To analyze the influence of the penetration rate of CAVs on the characteristics of the new mixed traffic flow at the curbside under different scenarios, we follow the procedure illustrated in Figures 8 and 9. This paper chooses the length of curbside as 240 m, 400 m, and 560 m in the simulation for small, medium, and large airport terminals, respectively. Referring to the study by Liu et al., we set the parking demand to 900 pcph, 1100 pcph, 1300 pcph, and 1500 pcph (where pcph = passenger cars per hour). These four demand levels cover scenarios ranging from "near saturation" to "severe oversaturation," ena-bling the analysis of capacity limits and delay patterns. Meanwhile, the CAV penetra-tion rates are set at 0%, 10%, 30%, 50%, 70%, and 100% [11].

Based on the survey by Liu et al., the vehicle composition at airport curbsides is 96% cars, 2% airport buses, and 2% regular buses [45]. To simplify the model, all vehicles in this simulation are cars. According to Table 1, parking times and vehicle speeds follow a normal distribution, with an average parking time of 105 s and a mean vehicle speed of 8 m/s. Vehicle arrivals follow a uniform distribution, with a maximum speed limit of 11.1 m/s on the curbside section. The length of the vehicle is set at 5 m, and the length of the parking space is set at 8 m.
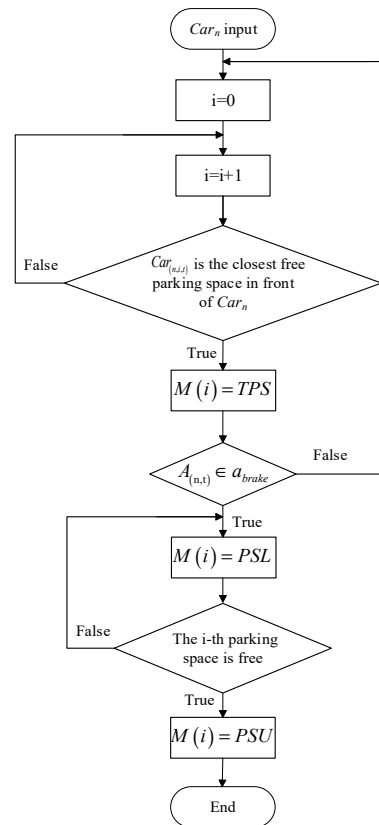
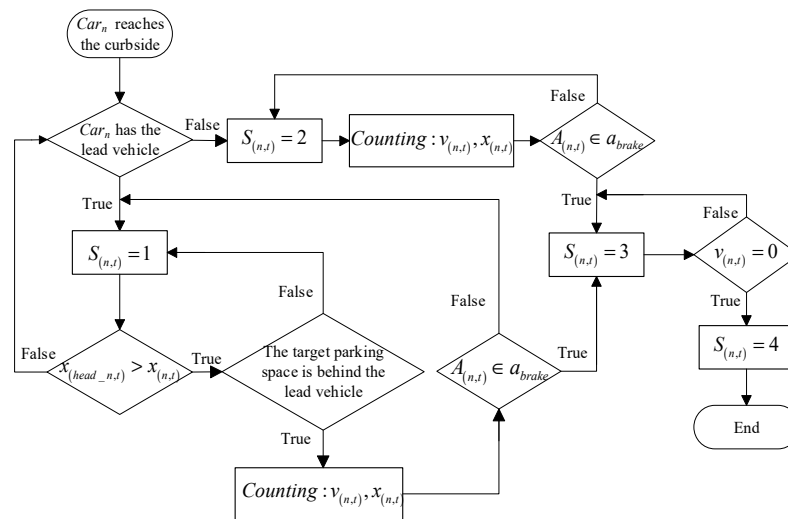**Figure 8.** The logic of the change in the status of the parking space.

Figure 9. The logic of parking simulation.

We divide the simulation principle into the vehicle parking principle and the vehicle departure principle. The principle of vehicle parking is shown in Figure 9. When the vehicle arrives at the curbside, it is recognized in ACF status or AFR status by determining whether there is a lead vehicle or not. There are two kinds of modes for vehicles to choose a parking space.

- The first mode is that the Car_n is in the AFR status. The Car_n updates its position and speed by constantly updating itself. When the $A_{(n,t)}$ of the Car_n is within the range of a_{brake}, the Car_n transitions to the AB status. Then, the final realization of braking and stopping occurs.

- The second mode is that the Car_n is in the ACF status. In this status, the Car_n is affected by the vehicle in front of it. The Car_n can only select a parking space between the vehicle in front and the Car_n for parking. When the status of the parking space selected by the Car_n changes to PSL. The Car_n performs braking and eventually stops.

The principle of vehicle departure is shown in Figure 10. The AP status of the vehicle is used as the starting point in the figure. When Car_n completes the parking service and satisfies the departure conditions (6) or (4), (7), and (9). The vehicle can enter the ride lane, and then Car_n leaves the curbside in ACF or AFR status. T_n is the Car_n's stopping time, $T_{(n,t)}$ denotes the time that Car_n has been parked at the moment of t, L denotes the length of the curbside.
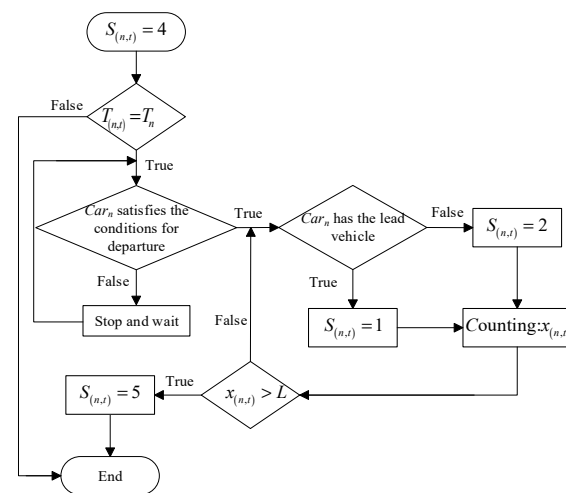

Figure 10. The logic of departure simulation.

4. Results and Discussion

We use MATLAB R2022b software to simulate three curbside lengths, four parking demands, and six CAV penetration rates, totaling 72 combinations. Based on the simulation results, we analyze the impact of CAV penetration rate on the curbside mixed traffic flow characteristics in terms of vehicle speed, delay time, and parking space occupancy, respectively.

4.1. Average Vehicle Speed Analysis

To intuitively demonstrate the impact of different penetration rates on overall vehicle speed under the same parking demand, we use a curbside length of 400 m as an example. The simulation stabilization period is chosen to last between 2000 s and 3000 s, as shown in Figure 11. In the figure, the vertical axis represents the average speed of all vehicles per second within the curbside length.

Figure 11 shows that for a fixed parking demand, the overall average speed of vehicles tends to increase as the penetration rate p rises. At low parking demand, the curve is denser, but when parking demand is greater than 1300 pcph, the curve gradually transitions from dense to sparse. To ensure accuracy of the results, we averaged the speeds of 1000 moments for each combination, representing the speed value for that combination. This allows us to compare the impact of different parking requirements on vehicle speed under the same penetration rate. The results of the calculations are shown in Figure 12.
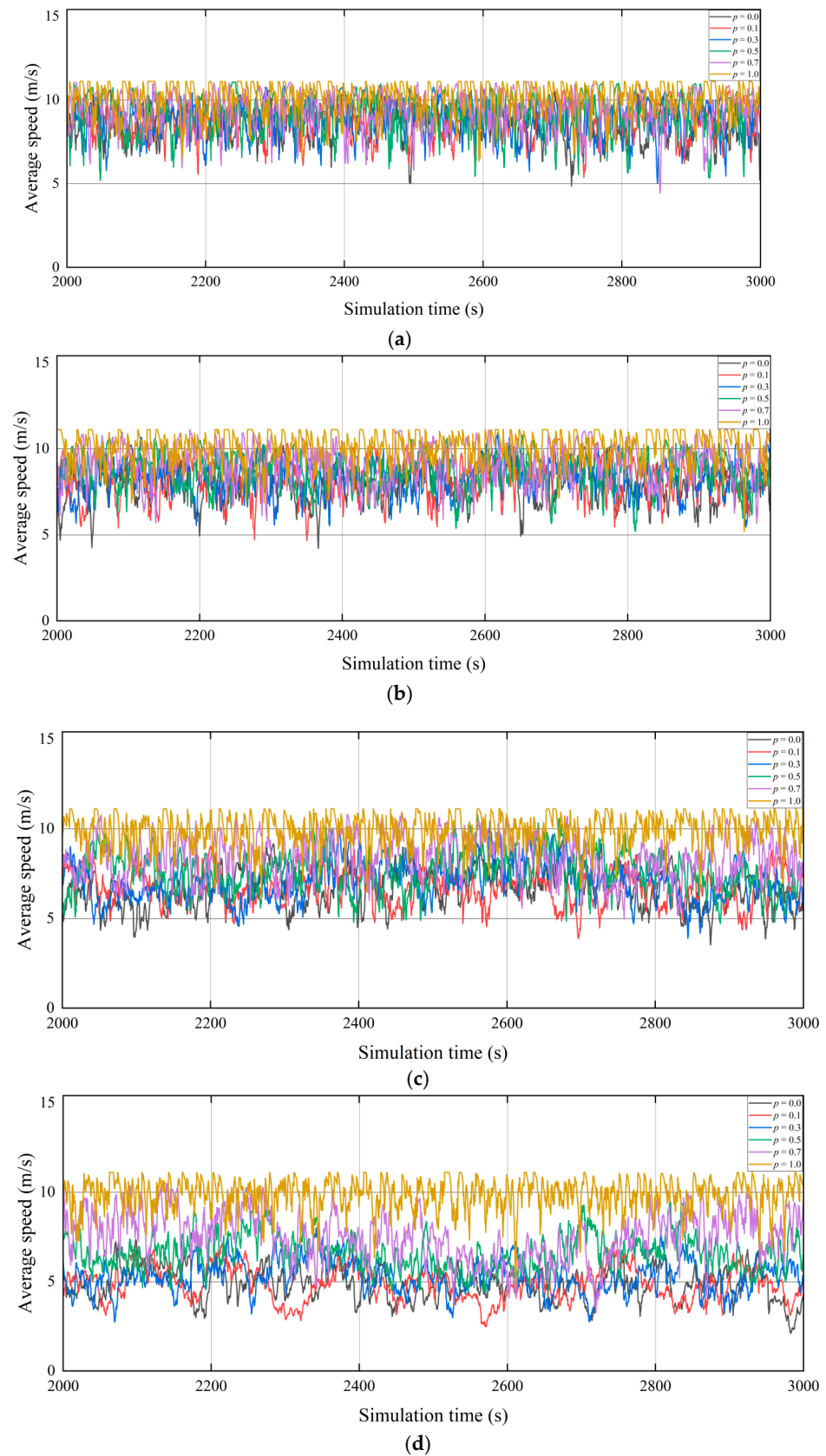
Figure 11. Results of the analysis of the average speed of vehicles. (**a**) 900 pcph, (**b**) 1100 pcph, (**c**) 1300 pcph, (**d**) 1500 pcph.

Figure 12 shows the existence of two phenomena for three curbside lengths. Under the same parking demand, as the penetration rate p increases, the average speed value shows

an increasing trend. Moreover, the greater the parking demand, the greater the increase in the average speed value, which means that the overall traffic efficiency of the vehicle is improved more effectively. In Figure 12b, we compare the average speed at p = 1 with that at p = 0 for different parking demands. When the parking demands are 900 pcph, 1100 pcph, 1300 pcph, and 1500 pcph, the overall traffic efficiency of the vehicle is improved by 16.83%, 25.51%, 48.69%, and 83.59%, respectively. Since the average velocity values all float around 10 m/s at p = 1, the magnitude of traffic efficiency improvement depends on the traffic situation at p = 0. At the same penetration rate p, with the increase in parking demand, the average speed value shows a decreasing trend. Moreover, with the increase of penetration rate p, the average speed value tends to be close to the state for different parking demands. To exemplify this phenomenon, we calculated the maximum difference in average speed for different parking demands. The results are summarized in Table 5. The addition of the CAVs optimizes the operational efficiency of the traffic flow. As the penetration rate p increases, when the penetration rate p is 1, as the homogeneous traffic flow of CAVs, there is no major difference in the overall average speed of the traffic flow under different parking demands. This is of great help in solving the congestion situation in the terminal building, where the curbside presents different congestion for different traffic volumes.
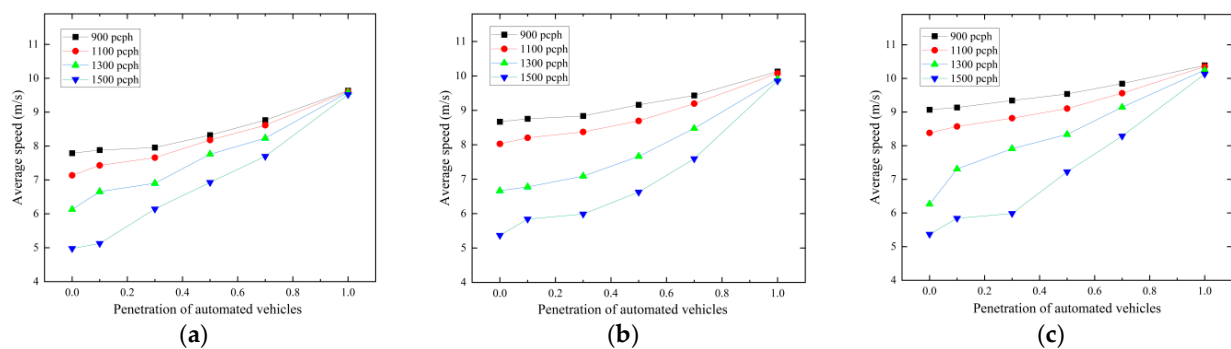

Figure 12. Analysis of average vehicle speed results for different combinations. (**a**) 240 m, (**b**) 400 m, (**c**) 560 m.

Table 5. Maximum difference in average velocity at the same permeability rate.

Penetration Rate p	Maximum Difference in Average Speed for Different Parking Demands		
	240 m	400 m	560 m
p = 0	2.81 m/s	3.30 m/s	3.70 m/s
p = 0.1	2.76 m/s	2.91 m/s	3.29 m/s
p = 0.3	1.81 m/s	2.85 m/s	3.36 m/s
p = 0.5	1.39 m/s	2.54 m/s	2.31 m/s
p = 0.7	1.07 m/s	1.84 m/s	1.56 m/s
p = 1.0	0.11 m/s	0.27 m/s	0.26 m/s

4.2. Analysis of Vehicle Delays

Delay is defined as the portion of time that the driver's real travel time exceeds the time spent traveling at the desired speed. Vehicles' delay times are affected in various respects. For example, vehicles are affected by the car-following model: when the vehicle decelerates, the rear vehicle follows the status change of the front vehicle to make corresponding measures. The deceleration causes the occurrence of vehicle delays, and braking behavior directly affects vehicle speed. According to the definition, the delay in this paper is

expressed as Equation (12). We calculate the delay time for each vehicle, and using a curbside length of 400 m as an example, the delay times are illustrated in Figure 13.

$$T_{\mathrm{n}} = (t_n - ts_n + 1) - \frac{L}{V} \tag{12}$$

where T_{n} denotes the delay time of the n-th vehicle, t_n denotes the moment when the n-th vehicle leaves the curbside, ts_n denotes the moment when the n-th vehicle arrives at the curbside, L is the length of the curbside, and V is the desired speed.
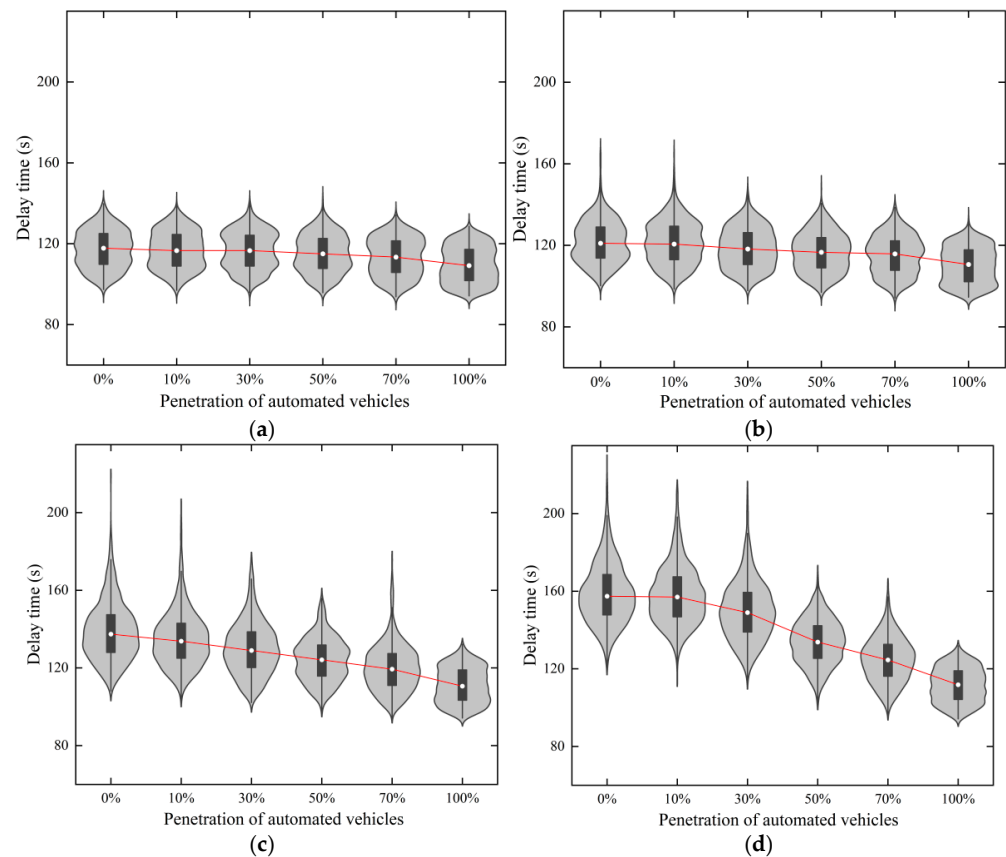

Figure 13. Results of the analysis of vehicle delay times. (**a**) 900 pcph, (**b**) 1100 pcph, (**c**) 1300 pcph, (**d**) 1500 pcph.

Figure 13 illustrates that the mean value of the overall vehicle delay time for a certain parking demand tends to decrease as the penetration rate p of CAVs increases. To further clarify the relationship between parking demand, penetration rate p, delay time, and average speed, we calculate the mean value of delay time under each combination. The results are shown in Figure 14.
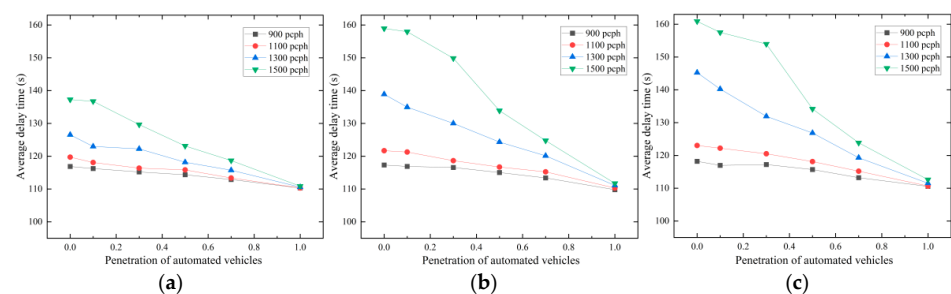

Figure 14. Analysis of vehicle delay time results for different combinations. (**a**) 240 m, (**b**) 400 m, (**c**) 560 m.

Figure 14 shows three key phenomena for different curbside lengths. Firstly, the average delay time of the vehicle as a whole shows a decreasing trend as the penetration rate p increases. This result, along with the findings in Figure 12, indicates that vehicle delay is inversely proportional to traffic efficiency. The average vehicle delays all fluctuate around 110 s at $p = 1$, which means that when the traffic flow is a homogeneous traffic flow of CAVs, the overall average vehicle delays converge under different lengths of curbsides, despite having different parking demands. This result verifies that the average speed floats around 10 m/s at $p = 1$ in Figure 12.

Comparing the scenarios at $p = 1$ with those at $p = 0$ for the four parking demands, the results of the calculations are shown in Table 6. From the results, the decrease in the average delay time shows an increasing trend as the length of the curbside increases for the same parking demand. This is because vehicles spend more time driving on longer curbside, making them more susceptible to the deceleration of the car-following model.

Table 6. Decrease in average delay time.

Parking Demands (pcph)	Decrease in Average Delay Time		
	240 m	400 m	560 m
900 pcph	5.62%	6.41%	6.46%
1100 pcph	7.84%	9.34%	10.05%
1300 pcph	12.60%	20.00%	23.22%
1500 pcph	19.22%	29.71%	30.00%

In terms of the effect of CAVs being able to reduce the vehicle delay time, this effect depends on the traffic condition at $p = 0$. In Figure 14b, when the parking demands are 900 pcph, 1100 pcph, 1300 pcph, and 1500 pcph at $p = 0$, the average vehicle delays are 117.32 s, 121.70 s, 138.89 s, and 158.94 s, respectively. The results indicate that the greater the parking demand, the greater the reduction in delay time. This may be caused by the fact that when parking demand is high, the changes in vehicle status within the mixed traffic flow are more complex and tend to cause congestion.

4.3. Parking Space Utilization Analysis

In Figure 11, although the increased penetration rate p of CAVs can improve the overall average speed of vehicles, the volatility of the average speed remains high, indicating that there is still congestion on the curbside. To explain this phenomenon, we analyzed the utilization of parking spaces in different scenarios. Since some parking demand cannot be met when the curbside length is 240 m, we calculate the utilization of parking spaces at the curbside lengths of 400 m and 560 m by using Equation (13). The results are shown in Figures 15 and 16.

$$P = \frac{\sum_{n=1}^{N} t'_n}{T} \tag{13}$$

where P denotes the parking space utilization rate, T denotes the period during which vehicles with parking demand use the curbside, N denotes the maximum number of parking spaces, and t'_n denotes the time at which the n-th vehicle occupies the parking space.

According to the simulation results, there are differences in the actual parking space utilization under different penetration rate scenarios once all vehicles have completed their parking demand. To maintain data consistency, we convert the number of parking spaces into a sequence of berth percentages on the horizontal axis. This method ensures that the endpoint of the horizontal axis is 1 for all scenarios, with the horizontal axis representing

the ratio of the individual parking space numbers to the total usage. Figures 15 and 16 show the general pattern for each combination under two curbside lengths.

As can be seen in the figure, the occupancy rate of the parking spaces is similar across various penetration rates p, indicating that traffic flows exhibit consistent characteristics in space occupancy under different scenarios (varying parking demands and penetration rates p), regardless of CAV involvement. The occupancy rate decreases as the berth percentage increases.
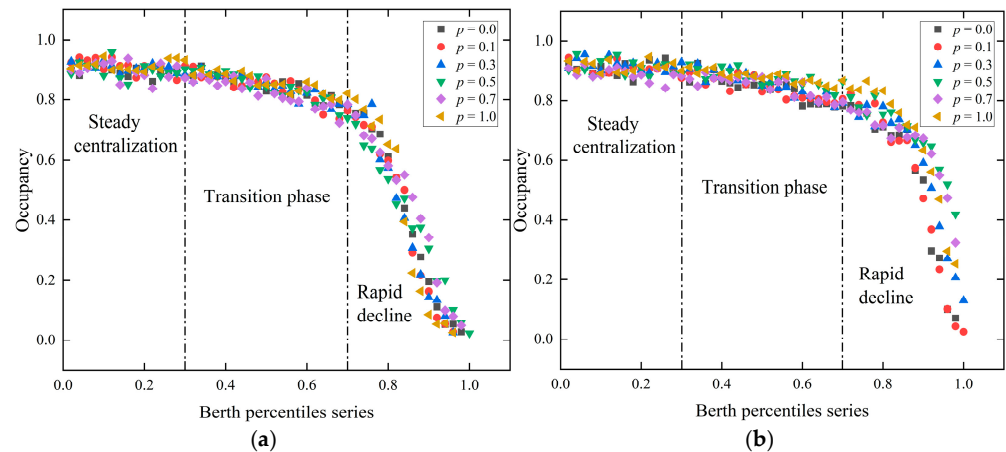

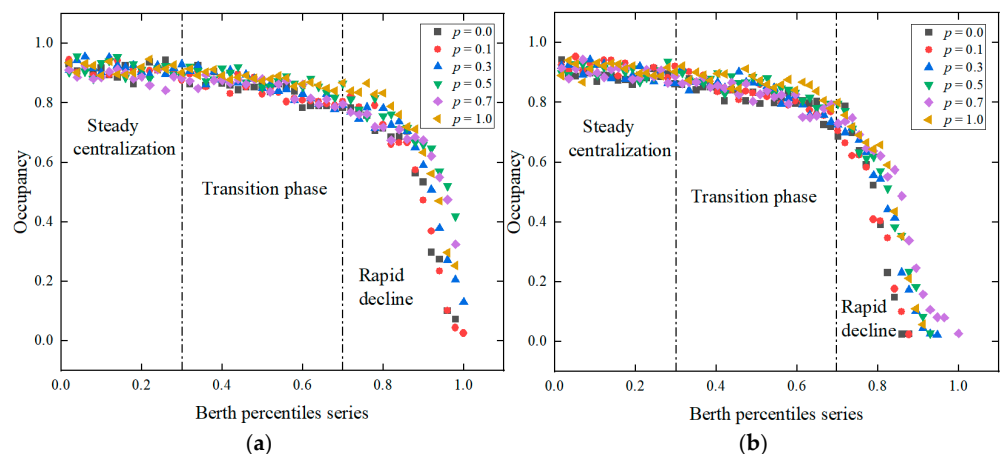**Figure 15.** Analysis of parking space utilization results at 1300 pcph. (**a**) 400 m, (**b**) 560 m.

Figure 16. Analysis of parking space utilization results at 1500 pcph. (**a**) 400 m, (**b**) 560 m.

This relationship between the berth percentage and the occupancy rate can be divided into three stages:

- First Stage (0–30% of berths): Occupancy is stable and concentrated.
- Second Stage (30–70% of berths): Known as the transition stage, occupancy shows a slow decreasing trend but remains high.
- Third Stage (70–100% of berths): Occupancy declines rapidly at a steady rate with a consistent slope.

In different scenarios, the mixed traffic flow with or without CAV vehicles exhibits similar characteristics in terms of parking space utilization. Among all the utilized parking spaces, the utilization rate is higher for the first 70%, with the utilization decreasing as the parking spaces get closer to the end of the curbside. Therefore, congestion in the mixed traffic flow tends to occur more frequently at the front end of the curbside, while it dissipates more easily as it moves towards the end of the curbside.

5. Conclusions

This paper proposes an innovative two-lane curbside parking simulation model, focusing on mixed traffic flows that include CAV vehicles. By constructing multi-type car-following models and integrating human driver behavior characteristics and safe lane-changing exit conditions. The model reproduces the dynamic process of vehicles arriving at the curbside, performing parking services, and departing from the curbside. The scientific contribution of this study lies in its systematic analysis of the traffic flow characteristics of CAVs and HDVs at airport terminal curbside, filling a critical gap in professional urban transportation environment research. Additionally, in light of the development trends in autonomous driving technology, this study not only provides theoretical guidance for airport curbside planning but also facilitates the transition of infrastructure toward autonomous driving technology. According to the analysis of the results, the main conclusions from the simulation results can be summarized as follows:

(1) CAVs can increase the traffic efficiency of mixed traffic flows: As the CAV penetration rate p increases, the average traffic efficiency of the mixed traffic flow gradually improves. Specifically, for a curbside length of 400 m and a parking demand of 1100 pcph. When the CAV penetration rate p is 10%, 30%, 50%, 70%, and 100%, respectively, the average traffic flow speed increases by 2.2%, 4.3%, 8.3%, 14.6%, and 25.5%, respectively, compared to $p = 0$. Meanwhile, when the CAV penetration rate p is 100%, the average traffic efficiency of the mixed traffic flow remains around 10 m/s in all scenarios.

(2) CAVs can significantly reduce vehicle delays: As the CAV penetration rate p increases, the vehicle delays in the mixed traffic flow are significantly reduced. Specifically, for a curbside length of 400 m and a parking demand of 1300 pcph. When the CAV penetration rate p is 10%, 30%, 50%, 70%, and 100%, respectively, vehicle delay time is reduced by 2.8%, 6.4%, 10.5%, 13.5%, and 20.0% compared to $p = 0$. Meanwhile, the increase in curbside length makes vehicles suffer more deceleration effects, which causes more delays. The average delay time of traffic flow fluctuates around 110 s when it is a homogeneous traffic flow of CAVs.

(3) The mixed traffic flow at different penetration rate p shows a consistent pattern in terms of parking space utilization: the occupancy rate decreases as the berth percentage increases. Specifically, it can be divided into three stages. The first stage (0–30% of berths) shows parking space utilization concentrated around 90%, exhibiting a stable and concentrated pattern. The second stage (30–70% of berths) sees parking space utilization fluctuating between 80% and 90%, showing a slow declining trend but still maintaining a high level. The third stage (70–100% of berths) experiences parking space utilization dropping below 80%, with a rapid decline at a stable rate and consistent slope.

(4) The average delay time of mixed traffic flow is inversely proportional to traffic efficiency: Under fixed curbside length and mixed traffic flow penetration rate p, as parking demand increases, the average traffic efficiency of the mixed traffic flow shows a decreasing trend, while the average vehicle delay time increases. Specifically, for a curbside length of 400 m and a penetration rate of $p = 0.3$, the average traffic efficiency of the mixed traffic flow is 8.8 m/s, 8.4 m/s, 7.1 m/s, and 6.0 m/s for parking demands of 900 pcph, 1100 pcph, 1300 pcph, and 1500 pcph, respectively. The average vehicle delay times are 116.6 s, 118.6 s, 130.0 s, and 149.9 s, respectively.

The simulation model used in this study assumes that vehicle acceleration, deceleration, and stopping behaviors are controlled by a simplified vehicle following model, ignoring some complex factors in actual traffic, such as individual differences among drivers, lateral vehicle movement, handling of sudden events, and the impact of weather conditions on traffic flow. In addition, this paper assumes that all vehicles follow the same rules and does not consider dynamic differences between different types of vehicles.

Future research can further explore the long-term impact of driver behavior and real-world roadside scenarios on mixed traffic flows, and optimize traffic flow management strategies to enhance overall efficiency:

(1) Research on driver behavior and technology interaction: Considering the individual differences among drivers and the impact of driving behavior on mixed traffic flows. Future research can introduce individualized driving models to examine the interaction between human drivers and CAVs on traffic flow, particularly changes in driving behavior under high CAV penetration scenarios.

(2) Multi-dimensional traffic flow simulation: Considering that real-world airport roadside environments may involve more complex factors, future research could expand the complexity of current models to include simulations of non-ideal conditions (such as weather, lighting, and traffic incidents), thereby enhancing the practical application value of simulation models.

Author Contributions: Writing—original draft, W.Y. and X.C.; Methodology, W.Y. and Z.L. (Zheng Liu); Supervision, Z.L. (Zhe Liu) and X.C.; Investigation, Y.T.; Writing—review & editing, Z.L. (Zhe Liu). All authors have read and agreed to the published version of the manuscript.

Data Availability Statement: The data that support the findings of this study are available on request from the corresponding author, Zhe Liu, upon reasonable request.

Conflicts of Interest: Author Zhe Liu was employed by the company China Highway Engineering Consultants Corporation, Ltd. The remaining authors declare that the research was conducted in the absence of any commercial or financial relationships that could be construed as a potential conflict of interest.

Abbreviations

The following abbreviations are used in this manuscript:

CAV	Connected autonomous vehicle
HDV	Human-driven vehicle
CACC	Cooperative adaptive cruise control
ACC	Adaptive cruise control
IDM	Intelligent driver model
CF	Car-following
ACF	Arriving and car-followed
AFR	Arriving and free-running
AB	Arriving and braking
AP	Arriving and parking
AL	Arriving and leaving
TPS	Target parking space
PSL	Parking space locking
PSU	Parking space unlocking

References

1. La Demanda Global del Transporte aéreo de Pasajeros Continuó Recuperándose en 2024. Available online: https://www.iata.org/en/pressroom/2025-releases/2025-01-30-01/ (accessed on 20 May 2024).
2. AlKheder, S.; Alhadeyah, S.; Albaghli, Z. Simulation modeling of passengers flow at airport terminals to reduce delay and enhance level of service. *Case Stud. Transp. Policy* **2024**, *18*, 101312. [CrossRef]
3. Scheelhaase, J.; Braun, M.; Maertens, S.; Grimme, W. Costs for passengers and airlines due to the significant delays and other irregularities at European airports in the 2022 summer season. *Transp. Res. Procedia* **2023**, *75*, 96–105. [CrossRef]

4. Gong, Z.; Zhang, F.; Liu, W.; Graham, D.J. On the effects of airport capacity expansion under responsive airlines and elastic passenger demand. *Transp. Res. Part B Methodol.* **2023**, *170*, 48–76. [CrossRef]

5. Parizi, M.S.; Braaksma, J.P. Optimum design of airport enplaning curbside areas. *J. Transp. Eng.* **1994**, *120*, 536–551. [CrossRef]

6. Lu, X.; Zhu, J.F.; Tang, X.W. Capacity assessment and optimization of terminal curbside. *J. Harbin Inst. Technol* **2009**, *41*, 96–99.

7. Zhang, Y. Analysis on dynamic capacity of curbside on transportation hub. *Technol. Econ. Areas Commun.* **2013**, *5*, 78–81.

8. Zhao, J.; Knoop, V.L.; Wang, M. Microscopic traffic modeling inside intersections: Interactions between drivers. *Transp. Sci.* **2023**, *57*, 135–155. [CrossRef]

9. Hu, Y.; Luo, X.; Bai, D. Passenger congestion alleviation in large hub airport ground-access system based on queueing theory. *Transp. B Transp. Dyn.* **2023**, *11*, 257–278. [CrossRef]

10. Chen, Y.; Zhang, N.; Wu, H.; Lu, Y.; Zhang, L.; He, J. Calculation Method of Traffic Capacity in Airport Curbside. In *Green Intelligent Transportation Systems, Proceedings of the 7th International Conference on Green Intelligent Transportation System and Safety 7, Online, 12 July 2017*; Springer: Singapore, 2018; pp. 725–736.

11. Liu, S.; Zhou, C.; Rong, J.; Ma, J.; Wang, Y. Measuring the length of a two-lane curbside based on traffic features. *Transp. Res. Rec.* **2020**, *2674*, 590–599. [CrossRef]

12. Harris, T.M.; Nourinejad, M.; Roorda, M.J. A mesoscopic simulation model for airport curbside management. *J. Adv. Transp.* **2017**, *2017*, 4950425. [CrossRef]

13. van Geelen, H.; Redant, K. Connected & Autonomous Vehicles and road infrastructure–state of play and outlook. *Transp. Res. Procedia* **2023**, *72*, 1311–1317.

14. Luo, S.; Zhang, S. Dynamic signal control for at-grade intersections under preliminary autonomous vehicle environment. *J. Cent. South Univ.* **2019**, *26*, 893–904. [CrossRef]

15. Yi, Z.; Lu, W.; Xu, L.; Qu, X.; Ran, B. Intelligent back-looking distance driver model and stability analysis for connected and automated vehicles. *J. Cent. South Univ.* **2020**, *27*, 3499–3512. [CrossRef]

16. Pan, Y.; Wu, Y.; Xu, L.; Xia, C.; Olson, D.L. The impacts of connected autonomous vehicles on mixed traffic flow: A comprehensive review. *Phys. A Stat. Mech. Its Appl.* **2024**, *635*, 129454. [CrossRef]

17. Gokasar, I.; Arisoy, A.A.; Deveci, M.; Mardani, A. Evaluation of a New Real-Life Traffic Management Using a Limited Number of Connected Autonomous Vehicles. *IEEE Trans. Intell. Transp. Syst.* **2023**, *25*, 3031–3040. [CrossRef]

18. Cao, Z.; Lu, L.; Chen, C.; Chen, X.U. Modeling and simulating urban traffic flow mixed with regular and connected vehicles. *IEEE Access* **2021**, *9*, 10392–10399. [CrossRef]

19. Yao, Z.; Ren, T.; Wang, Y.; Xu, Z.; Jiang, Y. Fundamental diagram of mixed traffic flow considering dedicated and shared lanes management policies for CAVs. *IEEE Trans. Transp. Electrif.* **2023**, *10*, 6964–6978. [CrossRef]

20. Ma, L.; Qu, S.; Ren, J.; Zhang, X. Mixed traffic flow of human-driven vehicles and connected autonomous vehicles: String stability and fundamental diagram. *Math. Biosci. Eng.* **2023**, *20*, 2280–2295. [CrossRef]

21. Yao, Z.; Hu, R.; Jiang, Y.; Xu, T. Stability and safety evaluation of mixed traffic flow with connected automated vehicles on expressways. *J. Saf. Res.* **2020**, *75*, 262–274. [CrossRef]

22. Sultana, T.; Hassan, H.M. Does recognizability of connected and automated vehicles (CAVs) platoons affect drivers' behavior and safety? *Transp. Res. Part F Traffic Psychol. Behav.* **2024**, *103*, 368–386. [CrossRef]

23. Amirgholy, M.; Nourinejad, M. Connected automated vehicles orchestrating human-driven vehicles: Optimizing traffic speed and density in urban networks. *Transp. Res. Part C Emerg. Technol.* **2024**, *165*, 104741. [CrossRef]

24. Cen, B.; Xue, Y.; Zhang, K.; Jia, L.; He, H.D. Study on traffic flows with connected vehicles and human-driven vehicles. *Appl. Math. Comput.* **2025**, *490*, 129182. [CrossRef]

25. Colovic, A.; Pilone, S.G.; Kukić, K.; Kalić, M.; Dožić, S.; Babić, D.; Ottomanelli, M. Airport access mode choice: Analysis of passengers' behavior in European countries. *Sustainability* **2022**, *14*, 9267. [CrossRef]

26. Nikhil, T.R.; Anusha, S.M. A critical review on transport planning analysis of airport connectivity-airport surface access. *Int. J. Sci. Res.* **2021**, *10*, 2277–8179.

27. Rassu, N.; Coni, M.; Maltinti, F. Analysis of the impact on the safety and sustainability of vehicular traffic in the landside area of Olbia-Costa Smeralda-airport. In *International Conference on Computational Science and Its Applications*; Springer: Cham, Switzerland, 2023; pp. 290–307.

28. Chen, C.C.F.; Schonfeld, P. Optimal clustering analysis for airport parking. *J. Air Transp. Manag.* **2024**, *120*, 102659. [CrossRef]

29. Yang, F.; Gu, W.; Cassidy, M.J.; Li, X.; Li, T. Achieving higher taxi outflows from a drop-off lane: A simulation-based study. *Transp. Res. Part C Emerg. Technol.* **2020**, *115*, 102623. [CrossRef]

30. Zhang, M.; Uno, N.; Yang, X. Traffic safety evaluation for mixed traffic flow caused by degradation of connected automated vehicles. *Phys. A Stat. Mech. Its Appl.* **2025**, *659*, 130353. [CrossRef]

31. Wang, Y.; Sun, L. Effects of safe driving climate among peers on the reckless driving behaviours of young drivers: The moderating effects of family climate and safety attitudes. *Transp. Res. Part F Traffic Psychol. Behav.* **2025**, *112*, 90–98. [CrossRef]

32. He, Y.; Hu, Y.; Li, J.; Sun, K.; Yin, J. Multi-scenario driving style research based on driving behavior pattern extraction. *Accid. Anal. Prev.* **2025**, *214*, 107963. [CrossRef]

33. Zhou, Z.; Li, L.; Qu, X.; Ran, B. A self-adaptive IDM car-following strategy considering asymptotic stability and damping characteristics. *Phys. A Stat. Mech. Its Appl.* **2024**, *637*, 129539. [CrossRef]

34. Wang, J.; Zhao, W.; Min, H.; Huang, Y.; Liu, C. String stability of the heterogeneous vehicle platoon considering connectivity uncertainty and autonomous driving levels under variable time headway strategy. *Transp. Lett.* **2025**, 1–22. [CrossRef]

35. Kim, B.; Heaslip, K.P. Identifying suitable car-following models to simulate automated vehicles on highways. *Int. J. Transp. Sci. Technol.* **2023**, *12*, 652–664. [CrossRef]

36. Bai, Y.; Tu, P.; Ong, G.P. An extended intelligent driving model for autonomous and manually driven vehicles in a mixed traffic environment with consideration to roadside crossing. *Int. J. Transp. Sci. Technol.* **2025**, *17*, 375–391. [CrossRef]

37. Chen, X.; Wu, Z.; Liang, Y. Modeling mixed traffic flow with connected autonomous vehicles and human-Driven vehicles in off-ramp diverging areas. *Sustainability* **2023**, *15*, 5651. [CrossRef]

38. Song, C.; Jia, H. Multi-State car-following behavior simulation in a mixed traffic flow for ICVs and MDVs. *Sustainability* **2022**, *14*, 13562. [CrossRef]

39. Zhang, T.T.; Jin, P.J.; McQuade, S.T.; Bayen, A.; Piccoli, B. Car-Following Models: A Multidisciplinary Review. *IEEE Trans. Intell. Veh.* **2024**, *10*, 92–116. [CrossRef]

40. He, Y.; Montanino, M.; Mattas, K.; Punzo, V.; Ciuffo, B. Physics-augmented models to simulate commercial adaptive cruise control (ACC) systems. *Transp. Res. Part C Emerg. Technol.* **2022**, *139*, 103692. [CrossRef]

41. Zhang, J.F.; Wan, Q.; Liu, Q.Q.; Xiao, Y.; Lv, B.; Tang, J.Y. Analyzing the Features of Passenger Drop-Off Behavior at Airport Curbsides: A Case Study From Guangxi Province, China. *IEEE Access* **2023**, *11*, 120209–120221. [CrossRef]

42. Chang, X.; Li, H.; Rong, J.; Zhao, X.; Li, A. Analysis on traffic stability and capacity for mixed traffic flow with platoons of intelligent connected vehicles. *Phys. A Stat. Mech. Its Appl.* **2020**, *557*, 124829. [CrossRef]

43. Ramireddy, S.; Ala, V.; Mehar, A. Acceleration and deceleration rates of various vehicle categories at signalized intersections in mixed traffic conditions. *Transp. Eng.* **2021**, *49*, 324–332. [CrossRef]

44. Chang, X.; Li, H.; Zhang, X.; Rong, J.; Zhao, X. Transition patterns of driving style from a traditional driving environment to a connected vehicle environment: A case of an extra-long tunnel road. *Transp. Res. Part F Traffic Psychol. Behav.* **2022**, *90*, 181–195. [CrossRef]

45. Liu, S.; Jian, R.; Zhou, C.; Weng, Z.; Wang, Y. Research on the Calculation Method of Terminal Curbside Length. In *CICTP 2019*; American Society of Civil Engineers: New York, NY, USA, 2019; pp. 2136–2146.